Hindawi
Advances in Civil Engineering
Volume 2023, Article ID 2753641, 15 pages
https://doi.org/10.1155/2023/2753641

Research Article

Micro to Nanolevel Stabilization of Expansive Clay Using Agro-Wastes

Mehmood Munawar,[1] Ammad H. Khan,[1] Zia U. Rehman,[1] Abdur Rahim,[1] Mubashir Aziz,[2,3] Sultan Almuaythir,[4] Bothaina S. I. A. El Kheir,[5] and Farhan Haider[6]

[1]*Department of Transportation Engineering and Management, University of Engineering & Technology, Lahore 54890, Pakistan*
[2]*Department of Civil and Environmental Engineering, King Fahd University of Petroleum and Minerals, Dhahran 31261, Saudi Arabia*
[3]*Interdisciplinary Research Center for Construction and Building Materials, King Fahd University of Petroleum and Minerals, Dhahran 31261, Saudi Arabia*
[4]*Department of Civil Engineering, Prince Sattam Bin Abdul Aziz University, Alkharj 16273, Saudi Arabia*
[5]*Department of Architectural Engineering, Faculty of Engineering and Technology, Future University, Cairo 11835, Egypt*
[6]*Onstructive Pvt. Limited, Lahore 54792, Pakistan*

Correspondence should be addressed to Ammad H. Khan; chair-tem@uet.edu.pk

Received 10 November 2022; Revised 4 January 2023; Accepted 28 March 2023; Published 19 April 2023

Academic Editor: Jiang Xiangang

The circular economy encourages the production and consumption of sustainable embankment geomaterials and their blends utilizing recycled waste materials in roads, railway tracks, airfields, and underground structures. Geomaterials comprising high-plastic soft expansive clay pose excessive settlement during cyclic traffic/railway/airfield loading resulting in uneven geometry of overlying layers. This paper demonstrates multiobjective optimized improvement of expansive clay (C) geotechnical characteristics by cost-effective agro-wastes additives at microlevel (by 3% to 12% rice husk ash, i.e., RHA), nanolevel (by 0.6% to 1.5% rice husk derived green nano-SiO_2, i.e., NS), and synergistic micro to nanolevel (NS-RHA). The swell potential, resilient modulus (MR), initial elastic modulus (Es), unconfined compressive strength (UCT), and California bearing ratio (CBR) of C and its blends were determined. The chemical characterization of C and its blends were conducted through Fourier transform infrared spectroscopy (FTIR) and optical microscopic tests. The outcome of this study depicted that the cost ratio for the optimized composite, i.e., (1.2% NS-9% RHA)/(9% RHA) is 1.22 whereas stiffness ratio MR (NS-RHA)/MR(RHA) and Es (NS-RHA)/Es(RHA) and strength ratio UCT(NS-RHA)/UCT(RHA) and CBR(NS-RHA)/CBR(RHA) were found to be 2.0, 1.64, 2.17, and 2.82, respectively. FTIR revealed the chemical compatibility between C, RHA, & NS from durability perspective. Cost-stiffness results of this study can be applied by geotechnical experts to economize the green stabilization of C by use of agro-waste for sustainable development.

1. Introduction

Sustainable embankment materials are desired globally by geotechnical experts from durability, cost-effectiveness, and optimization perspectives for civil engineering infrastructures [1–10]. Urbanization around the world is going on fast-track [11] due to which the problematic soils sites are also in demand for soils improvement (stabilization).

All soils from A-1 to A-7 (AASHTO classification) can be used as subgrades in pavements. High plasticity expansive clays are one of the common problematic soils that need the stabilization before its usage as bearing or construction material under embankments. These expansive clays are sufficiently strong in dry condition but with increase of moisture, these soils loose strength drastically [12, 13]. Expansive clay subgrade of low bearing capacity is considered as a costly issue [14] for which stabilization is

a feasible solution to increase shear strength and to decrease water susceptibility [15]. Furthermore, the expansive clays as subgrade are prone to large settlements resulting in formation of uneven geometry around the embankment [16–18]. From geotechnical perspectives in pavements subgrades built with expansive clays, commonly the more important parameters of interest are resilient modulus (MR), elastic modulus (Es), unconfined compressive strength (UCT), and California bearing ratio (CBR) index. MR is used in pavement design to simulate dynamic haversine traffic loading. Es estimated from stress-strain curve of UCT can be used for conservative design of pavements, [19] and it can be evaluated from straight line drawn at stress-strain curve up to 50% of peak stress [20]. CBR is the vital parameter which is used in the estimation of pavement thicknesses.

Flexible pavement components such as wearing course, base course, and subbase course usually have enough elasticity and transmit the overpassing vehicle loads to the underneath layer of expansive clay subgrade for dissipation [12, 13].

Traditional microstabilizers most notably cement, lime, and fly ash are in frequent use worldwide to improve expansive clay for the last few decades [21–24]. The main drawback of cement and lime stabilization is the emission of harmful gases such as CO_2, SO_2, and NO_x in the environment which outweighs their beneficial effects [25–27]. These microstabilizers increase the pH of expansive clay up to 12 which creates environmental problems [17]. Fly ash (a coal combustion product) due to its high value of the pH reduces the nutrient access to plants when mixed with expansive clays, so the adoption of green additives for stabilization is trending amongst geotechnical and pavement engineers [28–30].

Environmental friendly microstabilizers derived from agro-wastes are rapidly replacing the traditional microstabilizers for expansive clays [18]. Straw, bagasse, and husk are popular form of agro-wastes used. The increase in the use of expansive clays with agro-waste microstabilizers reduces the expenditure on cement which is being used earlier in abundance [12, 13]. Husk derived from rice (RH) showed promising potential for microstabilization of expansive clayey soils. Furthermore, the ash of rice husk (RHA) also proved potential for expansive clay stabilization at microlevel. RH is abundantly available in rice producing countries all over the globe as waste product of rice milling process. The chemical analysis shows that the 35% cellulose, 35% hemicellulose, 20% lignin and 10–20% ash can be obtained from of rice husk on dry weight basis [31]. RHA can be used as green additives due to its high pozzolanic activity [32]. RHA is produced by the burning of rice husk at about 600°C in which high quantity of silica, low quantity of oxide and high specific surface is observed.

The common nanoparticles used with soils are aluminium oxide-Al_2O_3, titanium oxide-TiO_2, silicon oxide-SiO_2, carbon nanotubes etc. These nanoparticles can stabilize (nanostabilization) the structure of soil at nanoscale (100 nm). The use of nanoparticles takes significance from the aspect of interparticle space concept, i.e., voids between soil particles. The nanoparticles cause transformation of pore liquid to viscous gel resulting in enhancement of soil shear resistance. The nanostabilization of soil improves its structure, physical, and chemical properties due to filling of voids at nanolevel [18]. In addition, the nanostabilization causes enhancement of load bearing potential of soil [33]. Various earlier researches described the interparticle spaces and potential of making the expansive clay denser with nanosilica.

The stabilization of soil at the microscale (using RH/RHA/cement/lime/fly ash/) does not change the properties of parent material significantly. Because, microstabilizers normally reduces plasticity of soils and facilitate in pozzolanic action. Nanostabilization is very active and changes the interlayer structure of parent soil and enhances the density and intermolecular attractive forces ultimately causing the increase in stiffness (resilient and elastic moduli) of blend. These nanoparticles influence the microstructure, physical, chemical, and geotechnical properties. Furthermore, the use of nanoparticles imparts the pozzolanic action in the blends.

Cost-effective and eco-friendly extraction of nanosilica from RHA can be accomplished by chemical and combustion methods. Reference [18] presented the combined effect of microlevel (cement) and nanolevel (nanosilica) on marl clay and found that nanosilica was four times more effective compared with cement stabilized marl clay.

The individual effects of nano and microparticles are needed to be compared with combined effect of nano plus microsynergy of particles. Previous studies present details of improvement in strength and plasticity of soft expansive clays by use of RHA and nano-SiO_2 independently. There are rare studies on the effect of synergistic combination (green and cost-effective) of micro and nanolevel particles on the resilient modulus (MR), elastic modulus (Es), UCT, and CBR of expansive clay. Followings were the objectives of the study:

(i) Evaluation of optimal doses of micro, nano, and micronano agro-waste additives for the synergistic green stabilization of expansive clay

(ii) Determination of optimal ratios of MR, Es, UCT, and CBR for nano to microlevel stabilization and comparison with cost ratio for nano to micro-synergistic mixing of RHA and NS in expansive clay

(iii) Characterization of expansive clay and its blends with RHA and NS through Fourier transform infrared spectroscopy (FTIR) and optical microscopic tests

2. Materials and Methods

Expansive clay samples (C) were characterized in the laboratory by specific gravity, natural moisture content, gradation, Atterberg limits, engineering classification, shear strength, consolidation, and modified proctor compaction tests. All tests were carried out in accordance with the relevant ASTM standards. Characterization of such types of clay has been described by Lang et al. [25]. The rice husk was collected from rice mill near Lahore, Pakistan. The rice husk

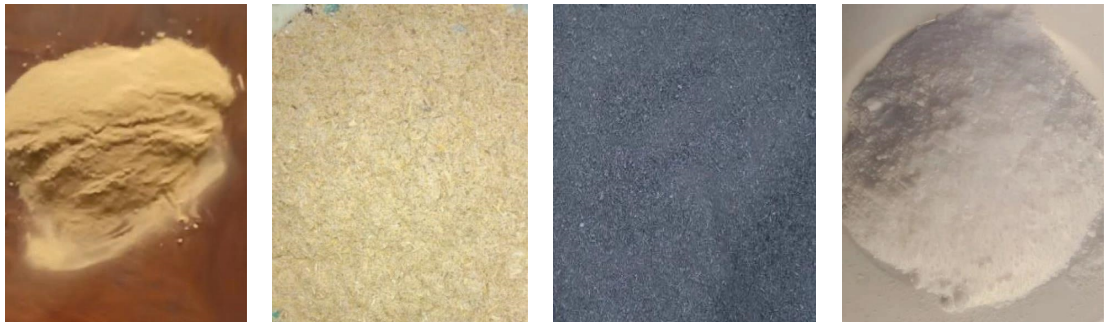

(a) (b) (c) (d)

Figure 1: Physical appearance of samples used (a) clay, (b) rice husk, (c) rice husk ash, and (d) nano-SiO_2.

was ground in 1000 rpm grinder for 4 minutes to prepare rice husk powder (RH). The particle sizes obtained ranged from 0.6 mm to 0.063 mm. The rice husk ash (RHA) was obtained by controlled burning of the RH at 600°C. RHA was characterized in the laboratory by the specific gravity, plasticity index, and loss-of-ignition tests. Commercially available nano-SiO_2 (NS) was procured. The properties of NS such as physical state, particle size, surface area, particles density, purity, and pH were determined in the laboratory.

Figure 1 shows the physical samples of clay, rice husk, rice husk ash, and nano-SiO_2 used.

RHA in the proportions of 3%, 6%, 9%, and 12% and NS in the proportions of 0.6%, 0.9%, 1.2%, and 1.5% were mixed in C to prepare samples for determination of swell potential, unconfined compressive strength (UCT), resilient modulus, and California bearing ratio (CBR). The proportion of RHA and NS was selected keeping in view the typical guideline range of these materials mixed with clay from previous studies [12–14, 32]. Tables 1–3 show the test matrix details used in experimentation.

C and its blends prepared with RHA and NS (Table 1) were subjected to evaluation of swell potential (ASTM D4546), unconfined compression (UCT) strength (ASTM D2166), resilient modulus (AASHTO T-307), and California bearing ratio (CBR) (ASTM D1883) tests. The length to diameter ratio of 2 was used in samples preparation. The strain rate of 1 mm/min in vertical axial direction was employed during UCT tests. The elastic modulus (Es) was derived from the initial portion of the stress-strain curves of UCT test. The peak stress, i.e., unconfined compressive strength (UCT), was also observed from the UCT stress-strain curves which depict the shear strength of the clay without any confining pressure. The resilient modulus (MR) test was performed on cyclic triaxial test machine. Cyclic haversine shaped load was applied for on each test specimen, and the last five cycles were selected for the measurement of load, horizontal deformation, and vertical deformation. In CBR tests, during saturation and shearing phases, a standard dead load of 10 lbs. was applied. The samples of C, C + RHA, C + NS, and C + RHA + NS prepared for UCT tests are shown in Figure 2.

Crystallographic structure of C and RHA was also evaluated by the X-ray diffraction (XRD) technique. The characteristics compositions of C, RH, RHA, NS, and C + RHA + NS (optimum blend) were also determined through the Fourier transform infrared (FTIR) spectroscopy and optical microscopy tests. The palettes of samples prepared for the FTIR tests are shown in Figure 3.

In order to compare the cost impact of different additives with clay, the stiffness to cost analysis was also carried out.

Table 1: Expansive clay plus rice husk ash composite tests matrix.

Sr	Label	Swell potential*	UCT*	Resilient modulus*	CBR*
1	C	X	X	X	X
2	C + 3%RHA	X	X	X	X
3	C + 6%RHA	X	X	X	X
4	C + 9%RHA	X	X	X	X
5	C + 12%RHA	X	X	X	X

Table 2: Expansive clay and nanosilica composite tests matrix.

Sr	Label	Swell potential*	UCT*	Resilient modulus*	CBR*
1	C + 0.6%NS	X	X	X	X
2	C + 0.9%NS	X	X	X	X
3	C + 1.2%NS	X	X	X	X
4	C + 1.5%NS	X	X	X	X

3. Results and Discussions

The geotechnical engineering characteristics of expansive clay are summarized in Table 4.

The C sample primarily comprised of fines, i.e., clay and silt in proportion of 73% and 23%, respectively. A fraction of 4% fine sand was also observed in the sample. The specific gravity of C was found 2.68 with plasticity index (PI) of 43%. The C was classified as medium to high-plastic clay (CH) in accordance with unified soil classification system (USCS). Such soils exhibit expansive nature, i.e., free swell potential 30% and swell pressure 232 kPa. The compression index of 0.44 was observed in C. The shear strength was found, i.e., cohesion of 61 kPa with friction angle of 100. The rice husk ash (RHA) and nanosilica characteristic properties are tabulated in Tables 5 and 6, respectively.

Table 3: Expansive clay, rice husk ash, and nanosilica composite tests matrix.

Sr	Label	Swell potential*	UCT*	Resilient modulus*	CBR*
1	C + 3%RHA + 0.6%NS	X	X	X	X
2	C + 3%RHA + 0.9%NS	X	X	X	X
3	C + 3%RHA + 1.2%NS	X	X	X	X
4	C + 3%RHA + 1.5%NS	X	X	X	X
5	C + 6%RHA + 0.6%NS	X	X	X	X
6	C + 6%RHA + 0.9%NS	X	X	X	X
7	C + 6%RHA + 1.2%NS	X	X	X	X
8	C + 6%RHA + 1.5%NS	X	X	X	X
9	C + 9%RHA + 0.6%NS	X	X	X	X
10	C + 9%RHA + 0.9%NS	X	X	X	X
11	C + 9%RHA + 1.2%NS	X	X	X	X
12	C + 9%RHA + 1.5%NS	X	X	X	X
13	C + 12%RHA + 0.6%NS	X	X	X	X
14	C + 12%RHA + 0.9%NS	X	X	X	X
15	C + 12%RHA + 1.2%NS	X	X	X	X
16	C + 12%RHA + 1.5%NS	X	X	X	X

*Average value of three replicates.

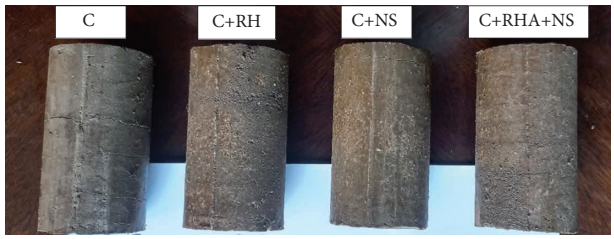

Figure 2: The UCT test samples of clay and its mixes.

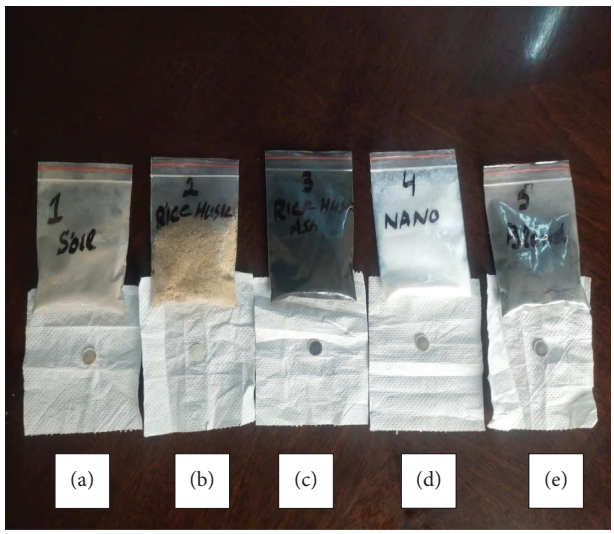

Figure 3: Palettes for the FTIR tests, i.e., (a) soil, (b) rice husk, (c) rice husk ash, (d) nanosilica, and (e) optimum blend of (a), (c), & (d).

The RHA exhibits dark grey color and nonplastic behavior with typical loss of ignition (LOI) value of 1%.

The nanosilica powder shows neutral behavior with an average particle density of 0.134 g/cm^2.

The effect of RHA and NS on free swell potential of clay is shown in Figure 4. It was observed that 3%, 6%, 9%, and 12% RHA caused 16%, 24%, 28%, and 32% decrease in swell potential of C. The C was also ameliorated with 0.6%, 0.9%, 1.2%, and 1.5% NS, which resulted in 24%, 40%, 44%, and 48% decrease in free swell potential. Moreover, the C was also blended with RHA plus NS composites. Synergistic composites of 3%, 6%, 9%, and 12% RHA with 0.6%, 0.9%, 1.2%, and 1.5% NS decreased the swell potential of C substantially as compared with the individual blends of C with RHA or NS as presented in Figure 4.

The optimal synergistic blend of 9% RHA plus 1.2% NS showed 72% decrease in free swell amongst studied proportions. The proportions blends showing the RHA and NS

Table 4: Summary of geotechnical engineering characteristics of expansive clay (C).

	Value^	Standard name
Constituent/property		
Specific gravity	2.68	ASTM D854
Natural moisture content (%)	22.5	ASTM D2216
Gradation/classification		
Sand (%)	4	ASTM D422
Silt (%)	23	ASTM D422
Clay (%)	73	ASTM D422
Atterberg limits		
LL-liquid limit (%)	91	ASTM D4318
PL-plastic limit (%)	49	ASTM D4318
PI-plasticity index (%)	43	ASTM D4318
SL-shrinkage limit (%)	39	ASTM D4318
USCS chart classification	CH	ASTM D2487
Cohesion (kPa)	61	ASTM 4767
Friction angle (degree)	10	ASTM 4767
Optimum moisture content (%)	24.3	ASTM D1557 ASTM D1557
Maximum dry density (g/cm^3)	1.74	ASTM 4546 ASTM4546
Free swell potential (%)	30	ASTM4546
Swell pressure (kPa)	232	ASTM4546
Compression index	0.44	

^Average value of three tests performed.

Table 5: RHA properties.

Properties	Percentage, %
Specific gravity	1.64
Color	Dark grey
Plasticity index (%)^	Nonplastic
Loss-on-ignition (%)^	1

^Average value of three tests performed.

Table 6: Physical properties of nano-SiO_2.

Parameters	Values
Physical state	Powder
Apparent particle size (nm)^	27 to 36
Specific surface area (m^2/g)^	187
Particle density (g/cm^3)^	0.134
Purity (%)	98.7
pH^	7

^Average value of three tests performed.

beyond 9% RHA and 1.2% NS presented higher free swell values due to dispersive effects of stabilizers.

The C was blended with different proportions of RHA, and it was observed that 3%, 6%, 9%, and 12% RHA caused 1.36, 1.66, 2.3, and 1.92 times increase in unconfined compressive strength (UCT). The C was also ameliorated with 0.6%, 0.9%, 1.2%, and 1.5% NS, which resulted in increase of 1.62, 2.23, 2.87, and 43 times UCT. Moreover, the C was also mixed with RHA plus NS composites. Synergistic composites of 3%, 6%, 9%, and 12% RHA with 0.6%, 0.9%, 1.2%, and 1.5% NS increased the UCT of C substantially as compared with the individual blends of C with RHA or NS as presented in Figure 5.

The combined effect of RHA and NS enhanced the UCT from 53 kPa (clay) to 265 kPa, i.e., 5 times higher, by the addition of optimized contents of 9% RHA and 1.2% of NS.

The stress-strain curves of UCT in Figure 6 show that the stress with respect to strain enhances the linear portion with increase in RHA and NS. The C was blended with different proportions of RHA, and it was observed that 3%, 6%, 9%, and 12% RHA caused 1.07, 1.17, 1.44, and 1.24 times increase in elastic modulus (Es) of clay. The C was also mixed with 0.6%, 0.9%, 1.2%, and 1.5% NS which caused an increase of 1.15, 1.28, 1.8, and 1.33 times the Es of C. Moreover, the C was also ameliorated by synergistic composites of RHA plus NS. Composites of 3%, 6%, 9%, and 12% RHA with 0.6%, 0.9%, 1.2%, and 1.5% NS increased the Es of C substantially as compared with the individual blends of C with RHA or NS as presented in Figure 6.

The combined effect of RHA and NS enhanced the Es from 54 MPa (native clay) to 128 MPa, i.e., 2.37 times as compared with C, by the addition of optimized contents of 9% RHA and 1.2% of NS.

The effect of RHA and NS on resilient modulus (MR) of clay is shown in Figure 7. The C was blended with different proportions of RHA, and it was observed that 3%, 6%, 9%, and 12% RHA caused 1.14, 1.2, 1.39, and 1.28 times increase in MR. The C was also ameliorated with NS which resulted in increase of 1.26, 1.43, 1.8, and 1.67 times increase in MR. Moreover, the C was also mixed with RHA plus NS composites. Synergistic composites of 3%, 6%, 9%, and 12% RHA with 0.6%, 0.9%, 1.2%, and 1.5% NS increased the MR of C substantially as compared with the individual blends of C with RHA or NS as presented in Figure 7.

The optimal synergistic blend of 9% RHA plus 1.2% NS presented the highest resilient modulus value in the studied blends, i.e., 2.79 times as compared with C. The proportions blends showing the RHA and NS beyond 9% RHA and 1.2% NS presented lower MR values due to dispersive effects of stabilizers as an effect of excessive quantities of RHA and NS. Past studies like Lang et al. [25] show that the addition of 1.5% nano-SiO2 to native clay soil presents lower strengths due to dispersive effects of excessive nanoparticles.

Increase in maximum dry density (γ_{dmax}) and decrease in optimum moisture content (OMC) were observed because of addition of RHA and NS. The increase in γ_{dmax} was seen as 20.7%, 29%, and 47.5% at optimized blends of 9% RHA, 1.2% NS, and 9% RHA plus 1.2% NS blends, respectively. Similar trends were observed in the case of soaked CBR values.

The C was blended with different proportions of RHA, and it was observed that 3%, 6%, 9%, and 12% RHA caused 1.04, 1.15, 1.28, and 1.19 times increase in CBR as shown in Figure 8. The C was also ameliorated with NS which resulted in increase of 1.23, 1.60, 1.85, and 1.43 times CBR as compared with C. Moreover, the C was also mixed with RHA plus NS composites. Synergistic composites of 3%, 6%, 9%, and 12% RHA with 0.6%, 0.9%, 1.2%, and 1.5% NS increased the CBR of C substantially as compared with the individual blends of C with RHA or NS as presented in Figure 8.

The synergistic optimized blend of 9% RHA plus 1.2% NS showed highest increase in CBR, i.e., 3.62 times higher than C.

The data were validated by statistical analysis and found in good health with no outliers.

Tables 7 and 8 summarized the chemical composition of native clay (C) and rice husk ash (RHA) observed through X-ray fluorescence analysis.

Both C and RHA materials primarily comprised of silica with 48.6% and 78.2%, respectively. Aluminum oxide was observed at 14.7% in C and 3.7% in RHA. Ferric oxide was found 8.4% in C and 1.1% in RHA. Sodium oxide was 3.1% in C while in RHA, it was 0.6%. In C, the potassium oxide was 0.67% while in RHA, it was 2.4%. 4.3% magnesium oxide was present in C, and 0.9% in RHA. Calcium oxide was 12.3% in C sample and 1.5% in RHA sample. All major compounds chemical composition in C and RHA samples were found common; hence, good affinity between both materials after mixing in blends was observed.

Figure 9 shows the individual Fourier transform infrared spectroscopy (FTIR) profiling of C, RH, RHA, NS and synergistic optimized blend of C with 9% RHA plus 1.2% NS. The peak pickings labelled 1 to 12 in the FTIR test results (Figure 9) were analyzed [34], and details of bonds, i.e., single, double, triple, and foot prints in C, RHA, NS, and synergetic optimum blend are summarized in Table 9. The

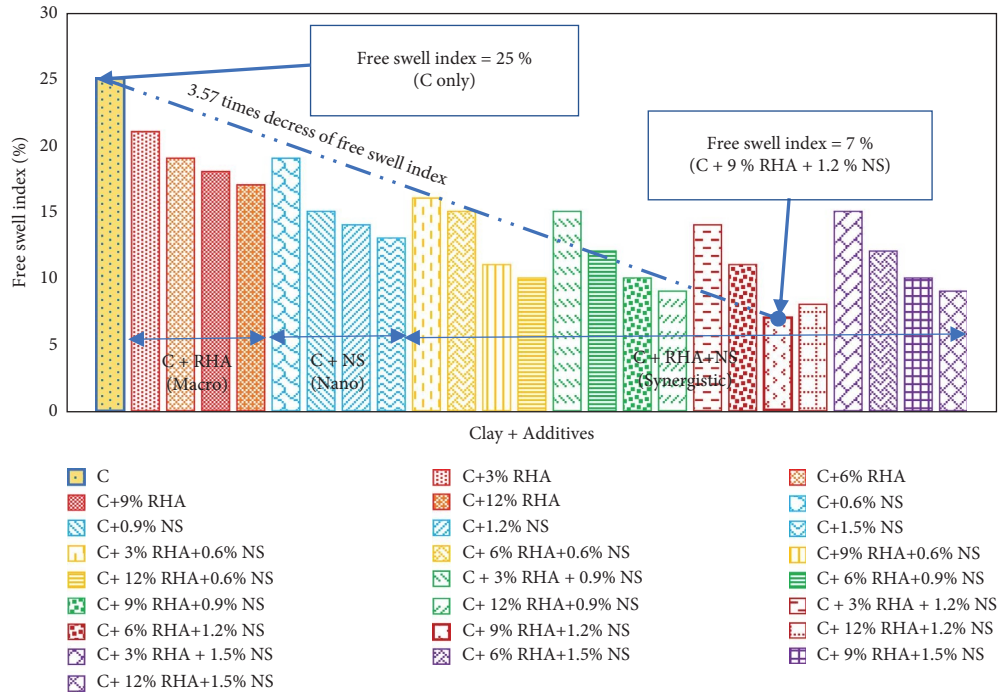

Figure 4: Free swell of clay and blends of clay plus RHA and NS synergistic.

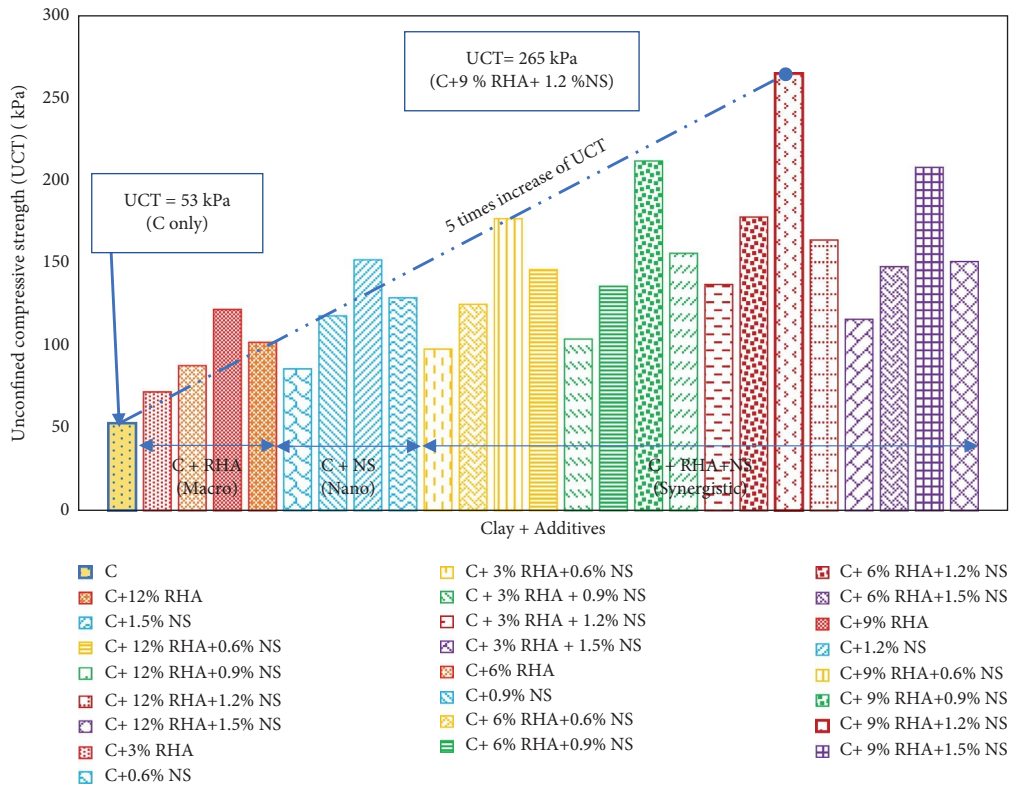

Figure 5: UCT of clay and blends of clay plus RHA and NS.

functional groups and their quantified frequencies were also determined for C, RHA, NS, and optimum blend [34].

The interpretation details of the FTIR results shown in Figure 9 and presented in Table 10 are explained as follows. In the range of 3650 and 3250 cm^{-1}, broad absorption bonds were observed in all samples showing the presence of hydrogen bond. Sharp bonds were observed round 3500 cm^{-1} regions in all samples illustrating the presence of oxygen

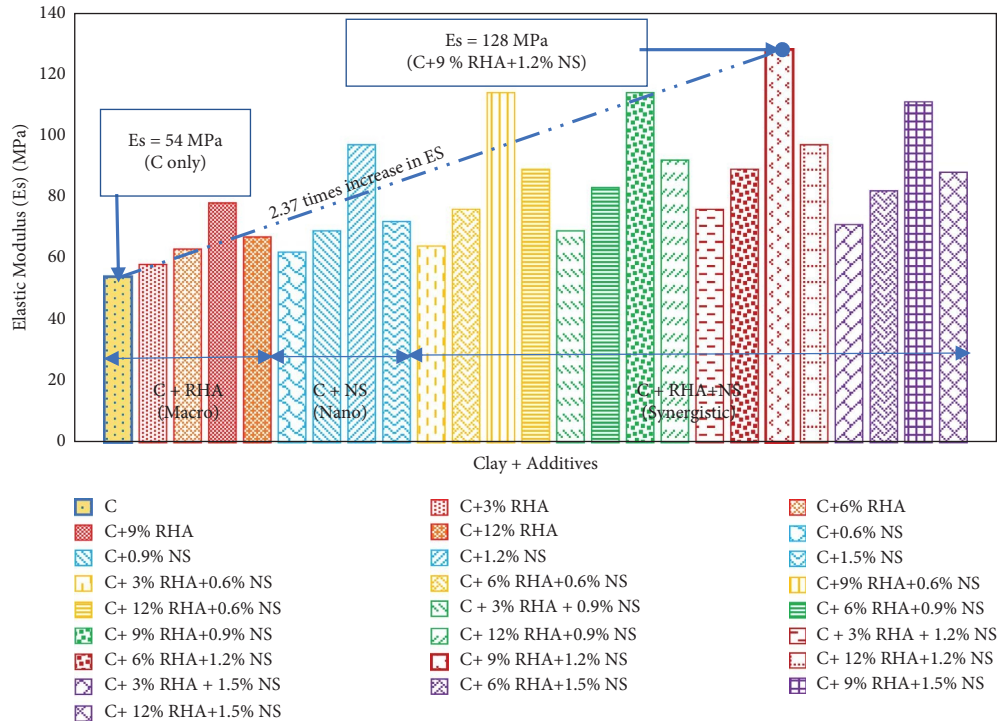

Figure 6: Es of clay and blends of clay plus RHA and NS.

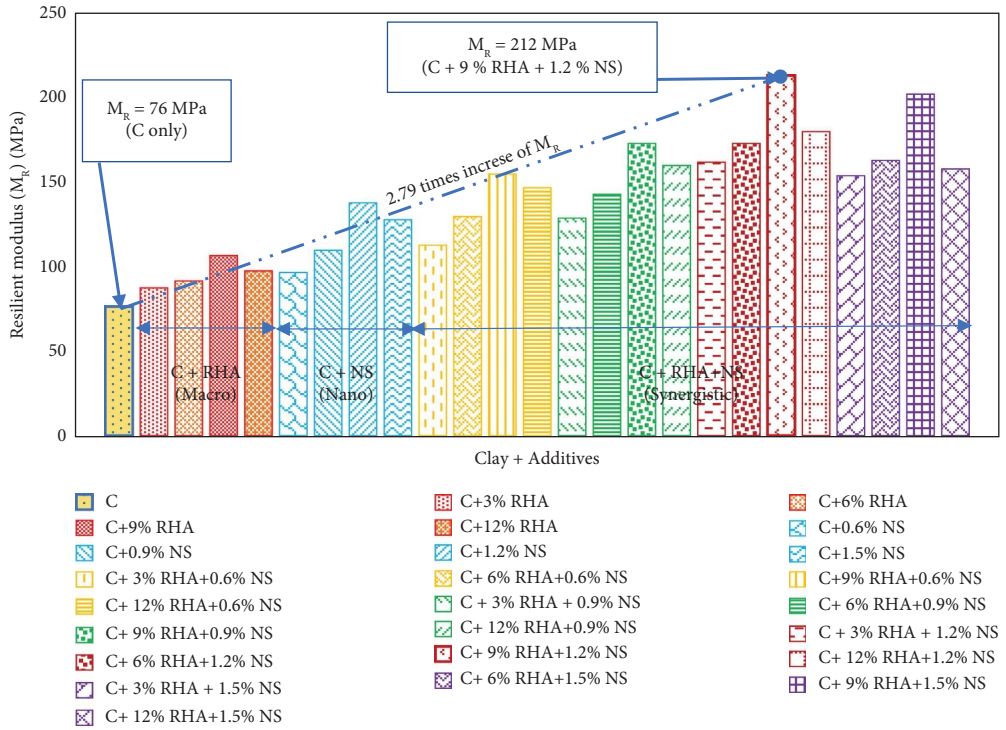

Figure 7: MR of clay and blends of clay plus RHA and NS.

related bonding. The peaks were observed in range of 3000 and 3200 cm^{-1} reflecting the presence of aromatic rings. Single bond of carbon (C-C) was observed in NS due to peak at 3000 cm^{-1}. No aldehyde peak was found in typical range of 2700 to 2800 cm^{-1}. No significant peaks were observed from 2000 to 2200 cm^{-1}, and hence, no carbon-carbon triple bond was observed in any samples. At about 1700 cm^{-1}, sharp peaks were observed in all samples demonstrating some carbonyl double bonds in the samples. At around 1600 cm^{-1}, peaks were observed in all samples informing the

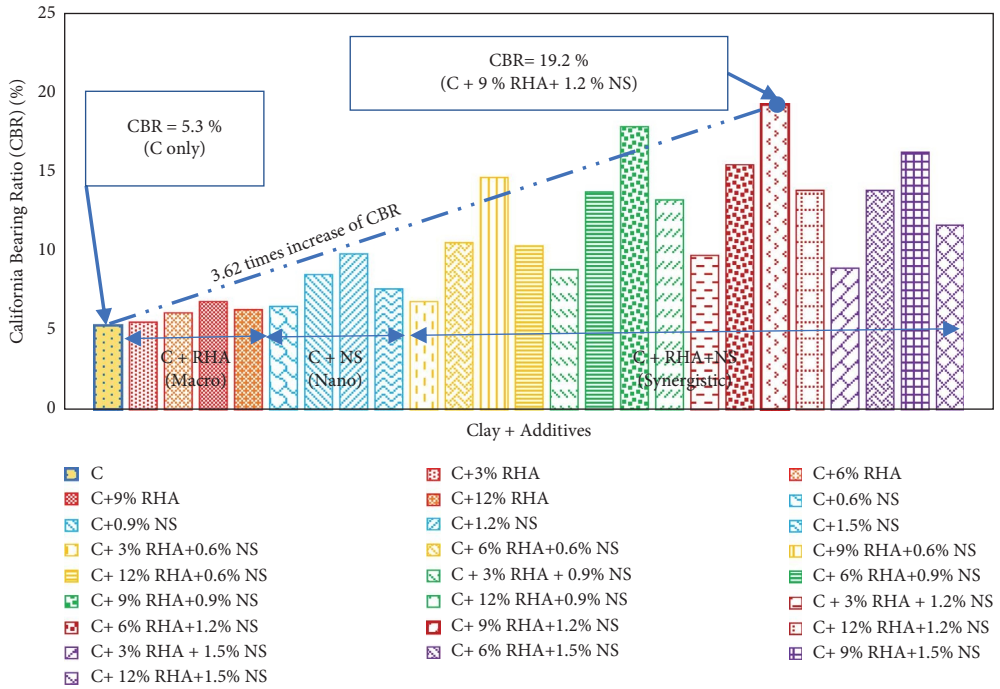

Figure 8: CBR of clay and blends of clay plus RHA and NS.

Table 7: Chemical composition of expansive clay (C) from X-ray (ASTM D5381) fluorescence analysis.

Constituents	Percentage, %
SiO_2-silica	48.6
Al_2O_3-aluminium oxide	14.7
Fe_2O_3- ferric oxide	8.4
MgO-magnesium oxide	4.3
CaO-calcium oxide	12.3
K_2O-potassium oxide	0.67
Na_2O-sodium oxide	3.1
Others	7.9

Table 8: Chemical composition of rice husk ash (RHA) from X-ray (ASTM D5381) fluorescence analysis.

Constituents	Percentage, %
SiO_2-silica	78.2
CaO-calcium oxide	1.5
Al_2O_3-aluminium oxide	3.7
Fe_2O_3-ferric oxide	1.1
Na_2O-sodium oxide	0.6
MgO-magnesium oxide	0.9
K_2O-potassium oxide	2.4
Others	11.6

presence of carbon-carbon double bond. At 1500 cm^{-1}, signals were observed showing the aromatic rings presence also in double bond region. Vinyl related compounds were also seen at about 1000 cm^{-1} in the finger print region. The similarity in peak trends was observed in all investigated materials showing comparable composition in spectrum and analysis regions (single bond, triple bond, double bond, and

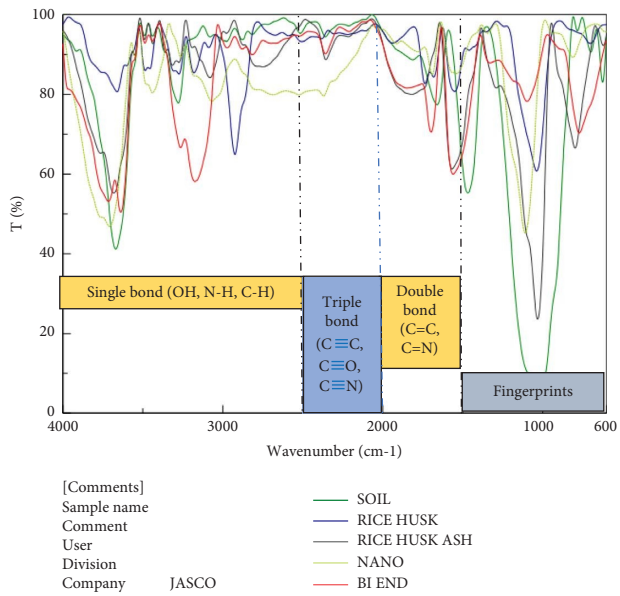

Figure 9: FTIR spectroscopy.

fingerprints). Out of all used materials and their combinations, i.e., C, RH, RHA, NS, and optimum blend, chemical compatibility was observed in FTIR spectroscopy except NS where single bond of carbon was observed in single bond analysis zone.

The optical microscopic images of C, RHA, NS, and C + RHA + NS optimal blend are presented in Figure 10. The optical images interpretation was carried out in accordance with guidelines of Pires et al. [36]. The results are summarized in Table 11. Pore size distribution (small, medium,

Table 9: The summary of FTIR tests analysis and wavenumber intensity and respective peak pickings.

Peak picking	1		2		3		4		5		6		7		8		9		10		11		12	
	W	T	W	T	W	T	W	T	W	T	W	T	W	T	W	T	W	T	W	T	W	T	W	T
C	3668	41	3278	77	2977	93	2358	94	1659	77	1467	55	1026	6	782	95	698	90	624	83	NA			
RHA	3681	55	3489	93	3437	92	3314	87	3080	84	2749	86	2355	88	1819	79	1566	61	1031	23	797	66	620	92
NS	3707	46	3549	89	3439	80	3262	89	3069	78	2370	79	1690	84	1538	85	1108	45	810	89	NA			
B	3715	53	3638	50	3487	92	3174	58	2814	98	2358	90	1697	70	1560	59	1098	78	771	70	NA			

W = wavenumber (cm^{-1}), T = transmittance (%).

Table 10: Interpretation of FTIR test results as per guidelines of Coates & Nandiyanto [34, 35].

Description	Spectrum	Analysis regions			
		Single bond (2500–4000 cm^{-1})	Triple bond (2000–2500 cm^{-1})	Double bond (1500–2000 cm^{-1})	Fingerprint (600–1500 cm^{-1})
C	Complex	(i)Hydrogen bond (ii)Oxygen related bonding (iii) Aromatic rings (iv) No aldehyde	(i) No carbon-carbon bond	(i) Carbonyl double bond (ii) Carbon-carbon double bond (iii) Aromatic rings	(i) Vinyl related compounds
RH	Complex	(i) Hydrogen bond (ii) Aromatic rings (iii) No aldehyde	(i) No carbon-carbon bond	(i) Carbonyl double bond (ii) Carbon-carbon double bond (iii) Aromatic rings	(i) Vinyl related compounds
RHA	Complex	(i) Hydrogen bond (ii) Oxygen related bonding (iii) Aromatic rings (iv) No aldehyde	(i) No carbon-carbon bond	(i) Carbonyl double bond (ii) Carbon-carbon double bond (iii) Aromatic rings	(i) Vinyl related compounds
NS	Complex	(i) Hydrogen bond (ii) Oxygen related bonding (iii) Aromatic rings (iv) No aldehyde (v) Single bond of carbon	(i) No carbon-carbon bond	(i) Carbonyl double bond (ii) Carbon-carbon double bond (iii) Aromatic rings	(i) Vinyl related compounds
C + 9%RHA + 1.2%NS blend	Complex	(i) Hydrogen bond (ii) Oxygen related bonding (iii) Aromatic rings	(i) No carbon-carbon bond	(i) Carbonyl double bond (ii) Carbon-carbon double bond (iii) Aromatic rings	(i) Vinyl related compounds

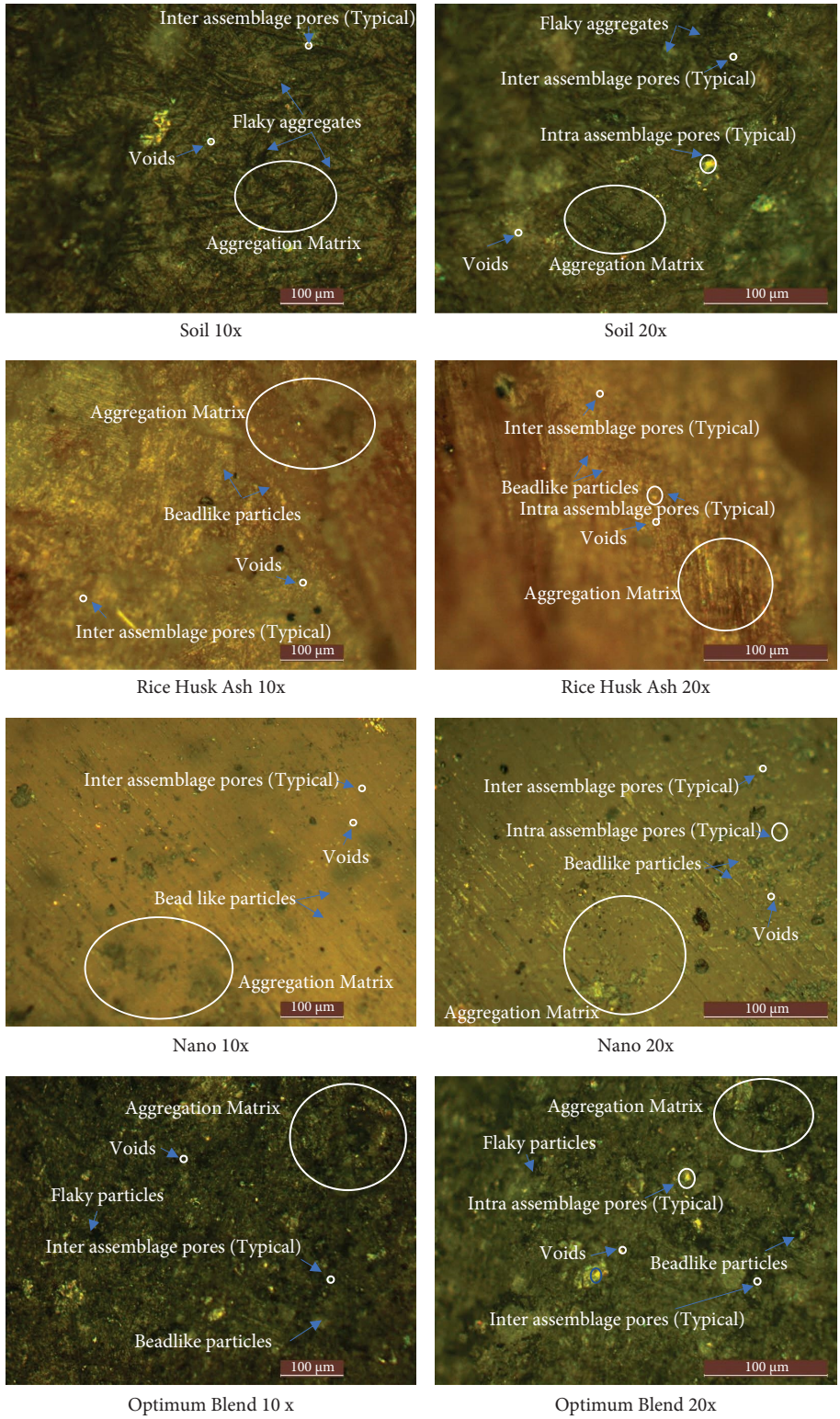

Figure 10: Optical microscopic images.

and large), irregularity (angular, flaky, and elongate), orientation (horizontal, circumferential, random), and macropore space and spatial distribution (bonded, intermediate, and elongated) were evaluated. Small to medium pore size distributions and voids were observed in the samples. In C and its optimal blend with RHA and NS, angular, flaky, and elongated fractions of irregularities were observed. The major orientation of RHA and NS being powders was observed circumferential/beadlike while C and its optimal blend exhibited a combination of circumferential/beadlike,

Table 11: Interpretation of optical image analysis results.

Description	Pore size distribution			Irregularity			Orientation			Space	Spatial distribution		
	Small	Medium	Large	Angular	Flaky	Elongated	Horizontal	Circumferential	Random	Macropore	Bonded	Intermediate	Elongated
C	—	X	—	X	X	X	X	X	X	X	X	X	X
RHA	X	X	—	—	—	—	—	X	—	X	X	—	—
NS	X	—	—	—	—	—	—	X	—	X	X	—	—
C + 9%RHA +1.2%NS	X	X	—	X	X	X	X	X	X	X	X	X	X

X denotes presence/yes.

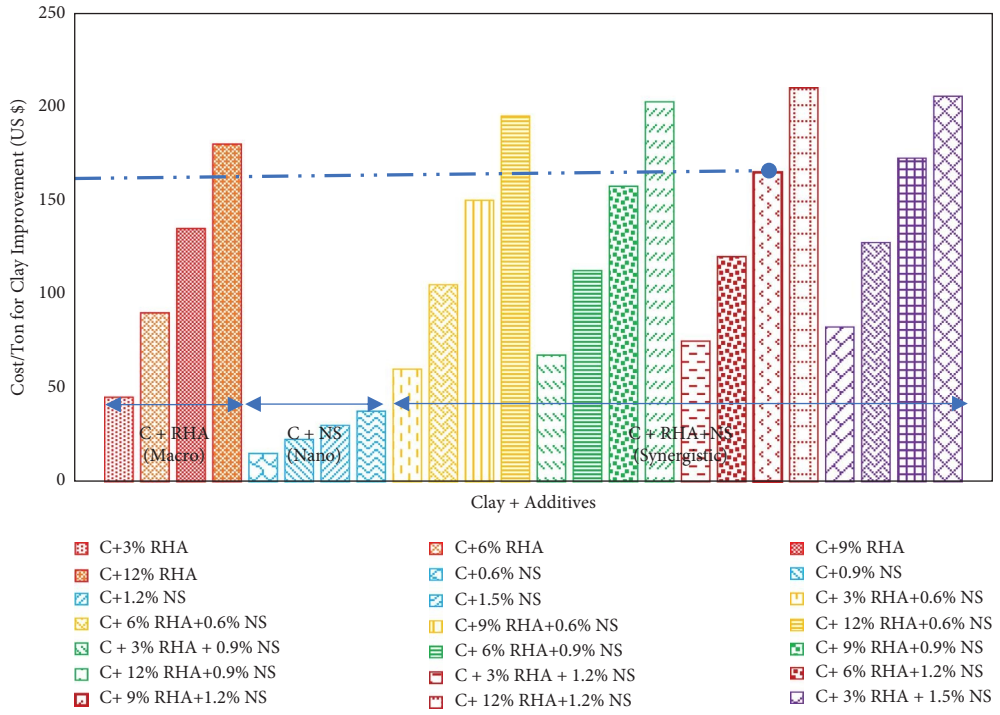

Figure 11: Cost versus stabilizer (RHA and NS) contents.

horizontal, and random orientations. Macropores can be seen in all samples marked as inter and intra-assemblage pores in Figure 10. The spatial distribution was observed in the form of aggregation matrix comprising of combination of bonded, intermediate, and elongated aggregates in C and its optimal blend. The RHA and NS, however, predominantly exhibited bonded spatial distribution.

The optical microscope analysis showed that clay stabilized with optimal dose of 1.2% of NS and 9% RHA exhibited optimum filling of pore spaces of native clay. Hence, the optimum values of density, stiffness, and strength parameters are validated.

The cost evaluation of microlevel stabilization (RHA) compared with nanolevel (NS) and micro plus nanolevel synergistic blends (C + RHA + NS) based on resultant optimal stiffness was carried out. The RHA and NS rates were used as \$1.5/kg and \$2.5/kg, respectively. In field, the cost of construction equipment, mixing, spreading, and compaction of both stabilizers, i.e., RHA and NS in expansive clay, is almost same. Hence, the cost analysis in this research only covered the cost of RHA and NS. The ratio of Cost(1.2%NS)/Cost(9%RHA) for individual stabilizers, i.e., NS and RHA, to achieve optimum stiffness and strength for treatment of one ton of clay, is \$30/\$135 = 0.22, whereas the optimal ratio for synergistic blend is Cost(1.2%NS–12%RHA)/Cost(12% RHA), i.e., \$165/\$135 = 1.22 which shows much higher enhancement in stiffness and strength of clay as the optimum ratios of MR (1.2%NS–9%RHA)/MR(9%RHA) = 2.0, Es (1.2%NS–9%RHA)/Es(9%RHA) = 1.64, UCT(1.2%NS-9% RHA)/UCT(9%RHA) = 2.17, and CBR(1.2%NS-9%RHA)/CBR(9%RHA) = 2.82. It was observed that the optimal blends of synergistic ratios show the RHA plus NS blends showing higher stiffness and strength ratios as compared with cost ratio of the corresponding blends. From Figures 5–8, it is observed that the ratio of MR (RHA-NS)/MR(RHA), Es (RHA-NS)/Es(RHA), UCT(RHA-NS)/UCT(RHA), and CBR(RHA-NS)/CBR(RHA) is 1.6, 1.3, 1.8, and 2.3 times higher than Cost(RHA-NS)/Cost(RHA), respectively, for optimal dose of 1.2% of NS plus 9% of microlevel RHA, validating the cost-effective solution for biocompatible stabilization of subgrade expansive clay.

It is observed from Figure 11 that for optimal blend of (1.2% NS + 9% RHA)/9% RHA, the ratio of cost for this blend is lower than the ratio of stiffness and strength parameters as presented in Figs. 5, 6, 7, 8. Beyond this optimal blend, the stiffness ratio decreases and the cost ratio increases making the blends uneconomical, e.g., 12% + 1.5% NS blend is uneconomical as it shows lower stiffness and strength ratios due to dispersive effects and higher cost ratio.

4. Conclusions

The purpose of this study was the sustainable stabilization of the high-plasticity expansive clay by green agro-waste additives at three levels, i.e., microlevel (by rice husk ash), nanolevel (by rice husk-derived nanosilica), and synergistic nano to microlevel (by blends of nanosilica and rice husk ash). FTIR, XRD, optical microscopic, and cost analysis were performed for each levels of stabilization for feasible blends evaluation to be used in amelioration of expansive clay. The following conclusions were addressed in this study:

(1) The optimal synergistic dose of micro to nanoparticles for stabilization of expansive clay was observed to be 1.2% of nanosilica (NS) and 9% of rice

husk ash (RHA) which resulted in improvement of resilient modulus (MR), elastic modulus (Es), unconfined compressive strength (UCT), and California bearing ratio (CBR) as 2.79, 2.37, 5.0, and 3.62 times, respectively, and free swell index was reduced up to 72% as compared with native expansive clay.

(2) The ratio of optimized contents for RHA, NS, and RHA-NS synergistic stabilization phases for MR, Es, UCT, and CBR are observed to be more than one, i.e., MR (RHA-NS)/MR(RHA), Es (RHA-NS)/Es(RHA), UCT (RHA-NS)/UCT(RHA), and CBR(RHA-NS)/CBR(RHA) as 2.0, 1.64, 2.17, and 2.82, respectively. Hence, it results in more sustainable stabilized mixes.

(3) The ratio of Cost(RHA-NS)/Cost(RHA) for optimal dose was evaluated as 1.22. The analysis also depicted that the ratio of MR (RHA-NS)/MR(RHA), Es (RHA-NS)/Es(RHA), UCT(RHA-NS)/UCT(RHA), and CBR(RHA-NS)/CBR(RHA) is 1.6, 1.3, 1.8, and 2.3 times higher than Cost(RHA-NS)/Cost(RHA), respectively, for optimal dose of 1.2% of rice husk-derived nanosilica plus 9% of microlevel rice husk ash, validating the cost-effective solution for biocompatible stabilization of subgrade expansive clay.

(4) The Fourier transform infrared spectroscopy (FTIR) revealed the chemical compatibility between C, RHA, & NS for possible future durability perspective. The optical microscope analysis showed that clay stabilized with optimal dose of 1.2% of NS and 9% RHA exhibited optimum filling of pore spaces of native clay. Hence, it validates the optimum values of density, stiffness, and strength parameters.

The study should be extended to explore the durability of the proposed blends. The optimization of the strength and durability is the function of C, RHA, and NS quantities of the blends.

Data Availability

The data supporting the current study are available from the corresponding author upon request.

Conflicts of Interest

The authors declare that they have no conflicts of interest.

Acknowledgments

This work was supported by the Higher Education Commission of Pakistan, NRPU 9631.

References

[1] A. H. Khan, Z. U. Rehman, and W. Abbass, "Prediction of post-yield strain from loading and unloading phases of pressuremeter, triaxial, and consolidation test curves for sustainable embankment design," *Sustainability*, vol. 14, p. 2535, 2022.

[2] W. Qamar, A. H. Khan, and Z. U. Rehman, "Sustainable application of wool-banana bio-composite waste material in geotechnical engineering for enhancement of elastoplastic strain and resilience of subgrade expansive clays," *Sustainability*, vol. 14, Article ID 13215, 2022.

[3] W. Chen, J. Zhao, L. Fan et al., "The effect of length and content of fiber on glass fiber and basalt fiber-reinforced granite residual soil," *Advances in Civil Engineering*, vol. 2022, no. 22, Article ID 7803002, 9 pages, 2022.

[4] Y. Liang, F. Zhang, M. Jing, and P. He, "Research on mechanical model of canal lining plates under the effect of frost heaving force," *Advances in Civil Engineering*, vol. 2022, no. 22, Article ID 8762382, 17 pages, 2022.

[5] W. Oueslati, C. Mejri, and A. B. H. Amara, "Impact of uniaxial mechanical perturbation on structural properties and smectite porosity features: ion exchanger efficiency and adsorption performance fate," *Advances in Civil Engineering*, vol. 2022, Article ID 4441705, 2022.

[6] D. Shewatatek, B. Tenaw, A. Yemiru, G. Belete, T. Tadesse, and T. Tolla, "Characteristics of sand at major quarrying areas around addis ababa," *Advances in Civil Engineering*, vol. 2022, Article ID 3198879, 9 pages, 2022.

[7] M. D. Bakare, R. R. Pai, S. Patel, and J. T. Shahu, "Environmental sustainability by bulk utilization of fly ash and GBFS as road subbase materials," *Journal of Hazardous, Toxic, and Radioactive Waste*, vol. 23, no. 4, 2019.

[8] B. A. Malik, P. Mandhaniya, and M. Y. Shah, "Experimental and numerical study on reinforcement of foundations using micropiles as a retrofitting measure," *Arabian Journal for Science and Engineering*, vol. 48, pp. 5335–5345, 2023.

[9] I. R. Sheikh, P. Mandhaniya, and M. Y. Shah, "A parametric study on pavement with geocell reinforced rock quarry waste base on dredged soil subgrade," *International Journal of Geosynthetics and Ground Engineering*, vol. 7, no. 2, p. 32, 2021.

[10] R. R. Pai, S. Patel, and M. D. Bakare, "Applicability of utilizing stabilized native soil as a subbase course in flexible pavement," *Indian Geotechnical Journal*, vol. 50, no. 2, pp. 289–299, 2020.

[11] E. A. Santos, C. T. D. S. Dutra, C. K. Chinelli, A. W. A. Hammad, A. N. Haddad, and C. A. P. Soares, "The main impacts of infrastructure works on public roads," *Infrastructure*, vol. 6, no. 9, p. 118, 2021.

[12] J. Karimiazar, M. Mahdad, and E. S. Teshnizi, "Assessing the geotechnical properties of soils treated with cement and nanosilica additives," *JOJ Science*, vol. 2, no. 3, pp. 56–59, 2020.

[13] J. Karimiazar, S. E. Teshnizi, and M. Mirzababaei, "California bearing ratio of a reactive clay treated with nano-additives and cement," *Journal of Materials in Civil Engineering*, vol. 34, no. 2, 2022.

[14] F. Buazar, "Impact of biocompatible nanosilica on green stabilization of subgrade soil," *Scientific Reports*, vol. 9, no. 1, 9 pages, Article ID 15147, 2019.

[15] K. Onyelowe, D. Bui Van, A. Eberemu et al., "Sorptivity, swelling, shrinkage, compression and durability of quarry dust treated soft soils for moisture bound pavement geotechnics," *Journal of Materials Research and Technology*, vol. 8, no. 4, pp. 3529–3538.

[16] A. Soltani, A. Taheri, M. Khatibi, and A. R. Estabragh, "Swelling potential of a stabilized expansive soil: a comparative experimental study," *Geotechnical & Geological Engineering*, vol. 35, no. 4, pp. 1717–1744, 2017.

[17] A. Ghorbani, H. Hasanzadehshooiili, M. Mohammadi et al., "Effect of selected nanospheres on the mechanical strength of

lime-stabilized high-plasticity clay soils," *Advances in Civil Engineering*, vol. 2019, Article ID 4257530, 11 pages, 2019.

[18] M. Mirzababaei, J. Karimiazar, E. Sharifi Teshnizi, R. Arjmandzadeh, and S. H. Bahmani, "Effect of nano-additives on the strength and durability characteristics of marl," *Minerals*, vol. 11, no. 10, p. 1119, 2021.

[19] J. E. Bowles, *Foundation Analysis and Design*, Wiley-Interscience, Hoboken, NJ, USA, 1996.

[20] R. D. Holtz, W. D. Kovacs, and T. C. Sheahan, *An Introduction to Geotechnical Engineering*, Prentice-Hall, Englewood Cliffs, NJ, USA, 2011.

[21] C. Olivier, A. Jean-Claude, and L. B. Tangi, "Microstructure and hydraulic conductivity of a compacted lime-treated soil," *Engineering Geology*, vol. 123, no. 3, pp. 187–193, 2011.

[22] B. Fatahi, T. M. Le, B. Fatahi, and H. Khabbaz, "Shrinkage properties of soft clay treated with cement and geofibers," *Geotechnical & Geological Engineering*, vol. 31, no. 5, pp. 1421–1435, 2013.

[23] S. M. S. Kazmi, S. Abbas, M. J. Munir, and A. Khitab, "Exploratory study on the effect of waste rice husk and sugarcane bagasse ashes in burnt clay bricks," *Journal of Building Engineering*, vol. 7, no. 9, pp. 372–378, 2016.

[24] J. Donrak, M. Hoy, and S. Horpibulsuk, "Environmental assessment of cement-stabilised lateritic soil/melamine debris for Thailand's pavement," *Environmental Geotechnique*, vol. 9, 2020.

[25] L. Lang, B. Chen, and N. Li, "Utilization of lime/carbide slag-activated ground granulated blast-furnace slag for dredged sludge stabilization," *Mineral Georesourse Geotechnology*, vol. 13, Article ID 1741050, 2020.

[26] K. Gu and B. Chen, "Research on the incorporation of untreated flue gas desulfurization gypsum into magnesium oxysulfate cement," *Journal of Cleaner Production*, vol. 271, Article ID 122497, 2020.

[27] L. Lang, B. Chen, and H. Duan, "Modification of nano-particles for the strength enhancing of cement-stabilized dredged sludge," *Journal of Rock Mechanics and Geotechnical Engineering*, vol. 13, no. 3, 2021.

[28] Y. Wang, P. Guo, and X. Li, "Behavior of fiber-reinforced and lime-stabilized clayey soil in triaxial tests," *Applied Sciences*, vol. 9, p. 900, 2019.

[29] S. G. F. P. Lemos, M. D. S. S Almeida, and N. C. Consoli, "Field and laboratory investigation of highly organic clay stabilized with portland cement," *Journal of Materials in Civil Engineering*, vol. 32, Article ID 04020063, 2020.

[30] H. Nasiri, N. Khayat, and M. Mirzababaei, "Simple yet quick stabilization of clay using a waste by-product," *Transportation Geotechnique*, vol. 28, Article ID 100531, 2021.

[31] B. S. Luh, *Rice: Production and Utilization*, AVI Publishing, CT, USA, 1980.

[32] J. Ma, Y. Su, and Y. Liu, "Strength and microfabric of expansive soil improved with rice husk ash and lime" Advances in Civil Engineering," vol. 2020, Article ID 9646205, 20 pages, 2020.

[33] O. Cuisinier, J. C. Auriol, T. Le Borgne, and D. Deneele, "Microstructure and hydraulic conductivity of a compacted lime-treated soil," *Engineering Geology*, vol. 123, no. 3, pp. 187–193, 2011.

[34] J. Coates, "Interpretation of infrar3d spoectra a practical approachEncyclopedia of analytical chemistry," *Infrared spectroscopy*, vol. 12, pp. 10815–10837, 2006.

[35] A. B. D. Nandiyanto, R. Oktiani, and R. Ragadhita, "How to read and interpret FTIR spectroscope of organic material," *Indonesian Journal of Science and Technology*, vol. 4, no. 1, pp. 97–118, 2019.

[36] L. F. Pires, F. S. Borges, S. Passoni, and A. Pereira, "Soil pore characterization using free software and a portable optical microscope," *Pedosphere*, vol. 23, no. 4, pp. 503–510, 2013.